

# Ion Chemistry of 1*H*-1,2,3-Triazole<sup>†</sup>

Takatoshi Ichino,<sup>‡</sup> Django H. Andrews,<sup>‡</sup> G. Jeffery Rathbone,<sup>‡</sup> Fuminori Misaizu,<sup>§</sup> Ryan M. D. Calvi,<sup>‡</sup> Scott W. Wren,<sup>‡</sup> Shuji Kato,<sup>‡</sup> Veronica M. Bierbaum,<sup>\*,‡</sup> and W. Carl Lineberger<sup>\*,‡</sup>

*JILA, University of Colorado and National Institute of Standards and Technology, Department of Chemistry and Biochemistry, University of Colorado, Boulder, Colorado 80309-0440, and Department of Chemistry, Graduate School of Science, Tohoku University, Aramaki, Aoba-ku, Sendai 980-8578, Japan*

*Received: June 21, 2007; In Final Form: August 30, 2007*

A combination of experimental methods, photoelectron-imaging spectroscopy, flowing afterglow-photoelectron spectroscopy and the flowing afterglow-selected ion flow tube technique, and electronic structure calculations at the B3LYP/6-311++G(d,p) level of density functional theory (DFT) have been employed to study the mechanism of the reaction of the hydroxide ion (HO<sup>-</sup>) with 1*H*-1,2,3-triazole. Four different product ion species have been identified experimentally, and the DFT calculations suggest that deprotonation by HO<sup>-</sup> at all sites of the triazole takes place to yield these products. Deprotonation of 1*H*-1,2,3-triazole at the N1–H site gives the major product ion, the 1,2,3-triazolide ion. The 335 nm photoelectron-imaging spectrum of the ion has been measured. The electron affinity (EA) of the 1,2,3-triazolyl radical has been determined to be 3.447 ± 0.004 eV. This EA and the gas-phase acidity of 2*H*-1,2,3-triazole are combined in a negative ion thermochemical cycle to determine the N–H bond dissociation energy of 2*H*-1,2,3-triazole to be 112.2 ± 0.6 kcal mol<sup>-1</sup>. The 363.8 nm photoelectron spectroscopic measurements have identified the other three product ions. Deprotonation of 1*H*-1,2,3-triazole at the C5 position initiates fragmentation of the ring structure to yield a minor product, the ketenimine anion. Another minor product, the iminodiazomethyl anion, is generated by deprotonation of 1*H*-1,2,3-triazole at the C4 position, followed by N1–N2 bond fission. Formation of the other minor product, the 2*H*-1,2,3-triazol-4-ide ion, can be rationalized by initial deprotonation of 1*H*-1,2,3-triazole at the N1–H site and subsequent proton exchanges within the ion–molecule complex. The EA of the 2*H*-1,2,3-triazol-4-yl radical is 1.865 ± 0.004 eV.

## Introduction

We recently initiated a research program to investigate the thermodynamic properties and the ion chemistry of a series of nitrogen-containing, five-membered ring, aromatic compounds, known as azoles. This systematic study is intended to elucidate the role of N atoms on the energetics of the heterocyclic molecules. Nitrogen-rich compounds have been recent research subjects as possible high energy-density materials.<sup>1–7</sup> We have previously studied azoles with one N atom (pyrrole<sup>8</sup>) or two N atoms (imidazole<sup>9</sup> and pyrazole<sup>10</sup>). In the present study, we explore the ion chemistry of 1*H*-1,2,3-triazole, which contains three adjacent N atoms in the five-membered ring (see Figure 1 for illustration).

By far the most acidic site of azoles is the N–H site, where deprotonation easily takes place when they react with the hydroxide ion (HO<sup>-</sup>). As the number of N atoms increases from one to two in the five-membered ring, we have also observed deprotonation at the C–H site in photoelectron spectroscopic measurements.<sup>9,10</sup> These observations indicate that the presence of an additional N atom affects the thermodynamic properties of the ring compounds such that not only the N–H site but also the C–H site becomes more acidic. Recently, we have further explored the thermochemistry of the C–H bonds in

imidazole and pyrazole experimentally, by substituting a methyl group for the H atom at the N–H site.<sup>11</sup>

The findings in these studies led us to speculate that 1*H*-1,2,3-triazole is even more acidic at both N–H and C–H sites than imidazole or pyrazole at the corresponding sites. If that is the case, then the reaction of HO<sup>-</sup> with the triazole becomes even more exothermic. This additional exothermicity will be available for the intermediate ion–molecule complex in the gas phase, and it is possible that this excess energy may induce further chemistry within the complex. For instance, DePuy studied the reactions of the vinylidiazomethyl anion with carbon dioxide (CO<sub>2</sub>), carbonyl sulfide (COS), and carbon disulfide (CS<sub>2</sub>),<sup>12</sup> where the exothermicity of the addition reaction increases in this order. As the exothermicity increases, more fragmented ion products were observed while fewer adduct ions were detected. There are a number of reports where multiple fragmentation pathways have been observed for highly exothermic negative ion reactions.<sup>12–18</sup>

In the present study, we utilize several experimental techniques to explore the mechanism of the reaction of HO<sup>-</sup> with 1*H*-1,2,3-triazole. More than one product ion species have been observed in mass spectroscopic measurements with a flowing afterglow-selected ion flow tube (FA-SIFT) instrument. We have previously demonstrated that a photoelectron spectroscopic technique is useful in identifying ion structures, particularly in distinguishing isomeric ions.<sup>9–11,19–22</sup> Four different product ions have been identified for the triazole reaction in photoelectron spectroscopic measurements. These products are the 1,2,3-triazolide ion, ketenimine anion, iminodiazomethyl anion, and

<sup>†</sup> Part of the “James T. (Casey) Hynes Festschrift”.

\* Corresponding authors. E-mail: (W.C.L.) wcl@jila.colorado.edu; (V.M.B.) veronica.bierbaum@colorado.edu.

<sup>‡</sup> University of Colorado.

<sup>§</sup> Tohoku University.

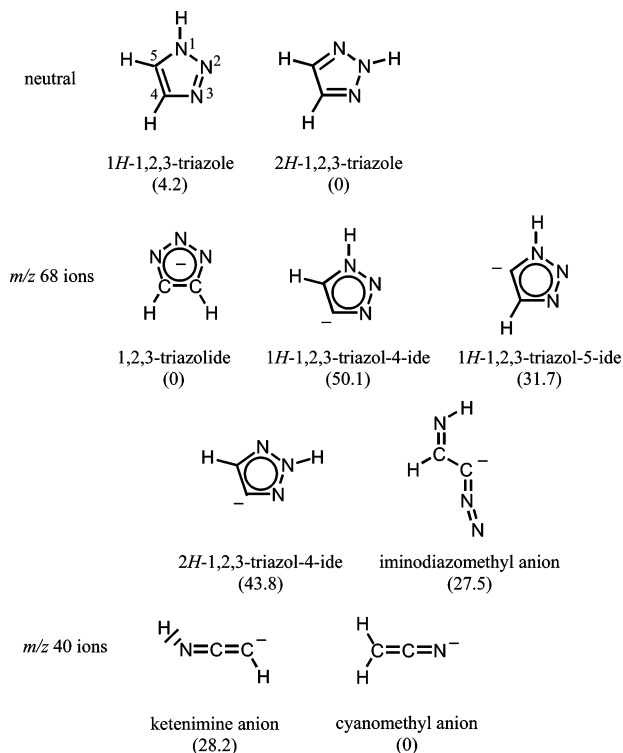


**Figure 1.** Structures of molecules studied in this work. The values represent the relative energies of the isomers evaluated with B3LYP/6-311++G(d,p) calculations (electronic energy + zero-point energy) in units of kcal mol<sup>-1</sup>.

2H-1,2,3-triazol-4-ide ion (Figure 1). Electronic structure calculations at the B3LYP/6-311++G(d,p) level of density functional theory (DFT) have been performed to elucidate formation of these ion species and better understand the reaction mechanism. These calculations support that HO<sup>-</sup> deprotonates 1H-1,2,3-triazole at all sites to induce chemical processes yielding these product ion species. The present study combines these experimental and theoretical techniques to reveal complexities of the reaction of HO<sup>-</sup> with 1H-1,2,3-triazole in the gas phase.

## Experimental Methods

**1. Flowing Afterglow-Selected Ion Flow Tube (FA-SIFT) Measurements.** The gas-phase reactivities of 1H-1,2,3-triazole and the 1,2,3-triazolide ion were studied at thermal energy (300 K) using a tandem FA-SIFT instrument.<sup>23,24</sup> The experimental procedures were analogous to those in previous studies.<sup>8–10</sup> 1H-1,2,3-triazole (C<sub>2</sub>H<sub>3</sub>N<sub>3</sub>, mp 23–25 °C, Aldrich, 97%) has only a very low vapor pressure at room temperature. For efficient introduction of the reagent into the instrument, a small flow of helium was bubbled through the liquid sample into the reaction flow tube. In the HO<sup>-</sup> deprotonation reaction of 1H-1,2,3-triazole, the HO<sup>-</sup> ions were generated in the source flow tube, mass-selected with a SIFT quadrupole mass filter, and injected into the second flow tube containing helium (0.5 Torr); the HO<sup>-</sup> ions were thermalized before reaction with the triazole, which is added downstream. In the gas-phase acidity bracketing experiments of the 1,2,3-triazolide ion, the *m/z* 68 ions were generated in the source flow tube using HO<sup>-</sup> deprotonation of 1H-1,2,3-triazole. The mass-selected *m/z* 68 ions were injected into the second flow tube at different injection energies (10–80 eV lab energy) and allowed to react with H<sub>2</sub>S or formic acid (HCOOH) added downstream. Reactant and product ions were analyzed using the detection quadrupole mass filter at the end of the second flow tube.

**2. Photoelectron-Imaging Spectroscopy.** The velocity map-imaging photoelectron spectrometer has been described in a previous publication.<sup>25</sup> The 1,2,3-triazolide ion is produced by electron impact ionization of a pulsed supersonic expansion.<sup>26</sup> An argon gas mixture containing 10% O<sub>2</sub> and 40% CH<sub>4</sub> is bubbled through heated liquid 1H-1,2,3-triazole (~80 °C) before passing through a supersonic expansion valve (General Valve Series 9). A 1 keV electron beam from an electron gun intersects the expansion to effect electron impact ionization. Following a drift time of <1 ms, the negative ions are extracted into a differentially pumped Wiley–McLaren time-of-flight mass spectrometer by a pulsed electric field. After mass selection, the ions are crossed with a pulsed laser (<200 μJ) from a frequency-doubled dye laser (335 nm) in a velocity map-imaging spectrometer. The three-dimensional photoelectron velocity distributions are reconstructed using the BASEX inversion algorithm.<sup>27</sup> The angular distribution of the photoelectrons follows<sup>28</sup>

$$I(\theta) = \frac{\sigma_0}{4\pi} (1 + \beta P_2(\cos \theta)) \quad (1)$$

where  $\theta$  is the angle between the electric field vector of the laser beam and the photoelectron momentum vector,  $\sigma_0$  is the total photodetachment cross section,  $\beta$  is the anisotropy parameter, and  $P_2(\cos \theta)$  is the second Legendre polynomial. The  $\beta$ -values are determined from the reconstructed image. The energy scale of the photoelectrons is calibrated in the measurements of the photoelectron spectrum of F<sup>-</sup>, utilizing the electron affinity (EA) of the F atom.<sup>29,30</sup>

**3. Flowing Afterglow-Photoelectron Spectroscopy.** The ultraviolet photoelectron spectrometer combined with a flowing afterglow negative ion source has been described in detail elsewhere.<sup>31–33</sup> A microwave discharge of helium buffer gas (~0.4 Torr) containing a small amount of O<sub>2</sub> produces the atomic oxygen ion (O<sup>-</sup>) in the ion source. A trace amount of methane is added downstream to convert O<sup>-</sup> to HO<sup>-</sup>. The HO<sup>-</sup> reacts with 1H-1,2,3-triazole introduced further downstream to form product ions, such as the 1,2,3-triazolide ion. Collisions with helium buffer gas thermalize the ions in the flow tube. The anions are extracted into a differentially pumped region, accelerated to 735 eV, and focused into a Wien velocity filter for mass selection. The mass-selected ion beam is refocused, decelerated to 35 eV, and overlapped with a laser beam in a high-vacuum build-up cavity for photodetachment. The output of a continuous wave argon ion laser (363.8 nm, 3.408 eV) is amplified in the cavity with a circulating power up to 100 W. A typical beam current for *m/z* 68 ions is 300 pA.

Photodetached electrons emitted into a small solid angle perpendicular to both the ion and laser beams are collected and focused into a hemispherical energy analyzer with a kinetic energy resolution of 8–10 meV. The energy analyzed photoelectrons are magnified onto the microchannel plates for amplification and imaged onto the position sensitive detector. The electron kinetic energy (eKE) settings for the analyzer are varied to construct spectra. The eKE is converted to the electron binding energy (eBE), which is equal to the difference between the laser photon energy and eKE. The absolute kinetic energy is calibrated in the measurements of the photoelectron spectrum of O<sup>-</sup> utilizing the EA of the O atom.<sup>29,30</sup> The energy scale is calibrated with a small (<1%) compression factor<sup>33</sup> that is derived in the measurements of the photoelectron spectra of O<sup>-</sup>, S<sup>-</sup>, and I<sup>-</sup> utilizing the EAs of the corresponding atoms.<sup>29,30</sup> A rotatable half-wave plate is inserted into the laser beam path before the build-up cavity to control the laser polarization

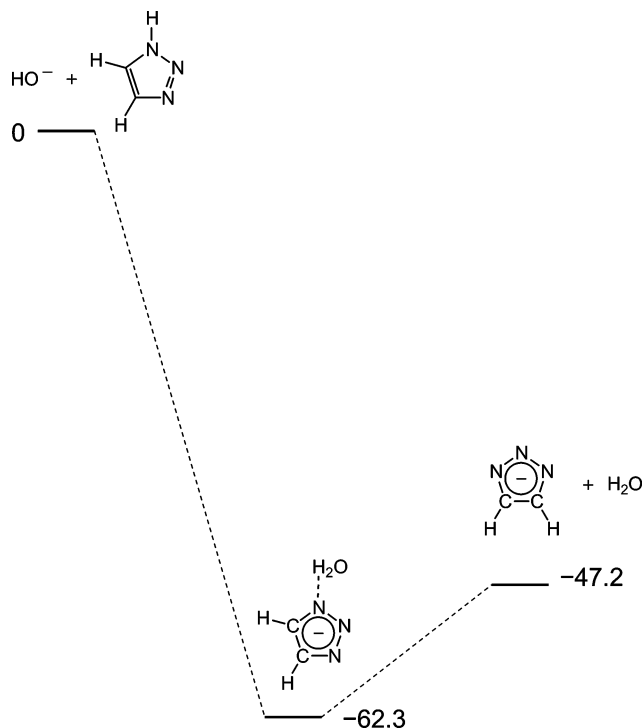


**Figure 2.** Energy diagram for the reaction of  $\text{HO}^-$  with 1*H*-1,2,3-triazole to produce the 1,2,3-triazolide ion. The 298 K enthalpies are evaluated with B3LYP/6-311++G(d,p) calculations. The values represent the 298 K enthalpies of the intermediate and final product states relative to that of the reactant state in units of  $\text{kcal mol}^{-1}$ .

direction and, consequently,  $\theta$  (see eq 1). Measurements at the magic angle ( $54.7^\circ$ ) provide photoelectron intensities uniformly proportional to  $\sigma_0$  (eq 1) at all kinetic energies. The  $\beta$ -values are determined by measuring the photoelectron counts as a function of  $\theta$ .

**4. Electronic Structure Calculations.** Electronic structure calculations were performed using the Gaussian 03 program package.<sup>34</sup> A variation of DFT, B3LYP,<sup>35,36</sup> was used with a basis set, 6-311++G(d,p).<sup>37</sup> The thermodynamic quantities were evaluated with the results of the DFT calculations. The zero-point energy corrections were also taken into account under the harmonic assumption. Harmonic frequencies were used without applying a scaling factor.

## Results and Discussion

**1. FA-SIFT Measurements on Proton-Transfer Reactions of 1*H*-1,2,3-Triazole and 1,2,3-Triazolide.** The reaction of  $\text{HO}^-$  with 1*H*-1,2,3-triazole produced  $m/z$  68 ions ( $\text{C}_2\text{H}_2\text{N}_3^-$ ) and  $m/z$  40 ions ( $\text{C}_2\text{H}_2\text{N}^-$ ) with an approximately 2:1 ratio. This result is in contrast to our findings for the reactions of  $\text{HO}^-$  with azoles containing one or two N atoms in the ring (i.e., pyrrole,<sup>8</sup> imidazole,<sup>9</sup> and pyrazole<sup>10</sup>) where only [M-H] ions (i.e., deprotonated ions) were observed as products.

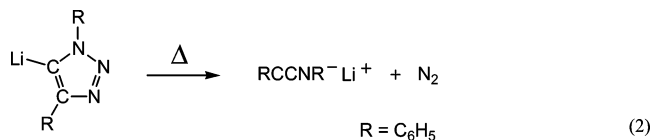
B3LYP/6-311++G(d,p) calculations suggest that  $\text{HO}^-$  deprotonation of 1*H*-1,2,3-triazole at the N1-H site, where the triazole is most acidic, is  $47.2 \text{ kcal mol}^{-1}$  exothermic. Analogous to the other azole systems, it is reasonable to assume that the 1,2,3-triazolide ion accounts for the majority of the  $m/z$  68 ions. Figure 2 shows the energy diagram for the N1-H deprotonation by  $\text{HO}^-$  evaluated by DFT calculations.

Acidity bracketing experiments were carried out for the  $m/z$  68 ions generated in the source flow tube. The  $m/z$  68 ions were SIFT-injected at a sufficiently low energy (20 eV) to minimize fragmentation. Negligible depletion of the  $m/z$  68 ions was

observed upon addition of  $\text{H}_2\text{S}$  whose gas-phase acidity is very accurately known;<sup>38,39</sup>  $\Delta_{\text{acid}}G_{298}(\text{H}_2\text{S}) = 344.9 \text{ kcal mol}^{-1}$ . On the other hand, rapid reaction of the  $m/z$  68 ions was observed upon addition of  $\text{HCOOH}$ , along with quantitative formation of  $\text{HCOO}^-$ . The gas-phase acidity of formic acid<sup>39-42</sup> is  $\Delta_{\text{acid}}G_{298}(\text{HCOOH}) = 338.2 \pm 0.4 \text{ kcal mol}^{-1}$ . These bracketing results show that the gas-phase basicity of the  $m/z$  68 ion is  $341.3 \pm 3.6 \text{ kcal mol}^{-1}$ .

In a Fourier transform-ion cyclotron resonance study, Catalán et al. conducted proton-transfer equilibrium measurements for the 1,2,3-triazolide ion with a few standard acids,<sup>43</sup> and their results indicate that the gas-phase acidity difference ( $\Delta\Delta_{\text{acid}}G_{298}$ ) between 2*H*-1,2,3-triazole and pyrrole is  $11.8 \pm 0.2 \text{ kcal mol}^{-1}$ . It should be noted that 2*H*-1,2,3-triazole is more stable than 1*H*-1,2,3-triazole in the gas phase,<sup>44</sup> and the proton-transfer equilibrium is established with respect to 2*H*-1,2,3-triazole instead of 1*H*-1,2,3-triazole. Because  $\Delta_{\text{acid}}G_{298}(\text{pyrrole})^8 = 351.9 \pm 0.4 \text{ kcal mol}^{-1}$ ,  $\Delta_{\text{acid}}G_{298}(2\text{H-1,2,3-triazole}) = 340.1 \pm 0.5 \text{ kcal mol}^{-1}$ . Thus, our acidity bracketing measurements support the inference that the  $m/z$  68 ions have primarily the 1,2,3-triazolide structure.

On the other hand, the identity of the fragmented ions of  $m/z$  40 is not clear. The concomitant neutral product must be  $\text{N}_2$ . Fragmentation of 1,2,3-triazole through anion chemistry in solution has been reported in the literature. Raap observed that 1,4-diphenyl-1,2,3-triazole can be lithiated easily at the C5 position at  $-20$  to  $-60^\circ\text{C}$ .<sup>45</sup> It was found that upon heating to room temperature the 1,4-diphenyl-1,2,3-triazolyl lithium rapidly fragments to  $\text{N}_2$  and lithium (*N*-phenyl)phenylketenimine anion.



The identity of this ion was confirmed by NMR and IR measurements following C-methylation. Analogous fragmentation processes for substituted 1,2,3-triazole systems can be found in the literature.<sup>45,46</sup>

We have explored a similar fragmentation process in the reaction of  $\text{HO}^-$  with 1*H*-1,2,3-triazole through DFT calculations. Figure 3 displays the summary of the computations for the fragmentation process.  $\text{HO}^-$  interacts with the triazole at the C5 position, and the resultant ion-molecule complex<sup>47</sup> is more stable than the reactants by  $33.4 \text{ kcal mol}^{-1}$ . Simple dissociation of the complex would lead to formation of the 1*H*-1,2,3-triazol-5-ide ion and  $\text{H}_2\text{O}$  with an overall exothermicity of  $15.5 \text{ kcal mol}^{-1}$ . The calculations also find, however, that the isolated 1*H*-1,2,3-triazol-5-ide ion can decompose into the ketenimine anion ( $m/z$  40) and  $\text{N}_2$  with an energy barrier<sup>48</sup> of  $16.2 \text{ kcal mol}^{-1}$ . The energy level for the transition state shown in Figure 3 is set by adding this energy barrier to the energy level of the ion-molecule complex. Because moderately large complexation energy is available, this fragmentation process seems probable in the reaction of  $\text{HO}^-$  with 1*H*-1,2,3-triazole.

**2. Photoelectron-Imaging Spectrum of the 1,2,3-Triazolide Ion.** The 335 nm photoelectron-imaging spectrum of  $m/z$  68 ions is shown in Figure 4. The spectrum exhibits an intense peak around eBE 3.45 eV, together with a number of peaks toward the higher eBE. The anisotropy parameters,  $\beta$  (eq 1), for all of the peaks observed in the spectrum are within the range of  $-0.2$  to  $-0.6$ .

The formation of the  $m/z$  68 ions in the ion source can be explained as follows. Electron impact ionization of the pulsed

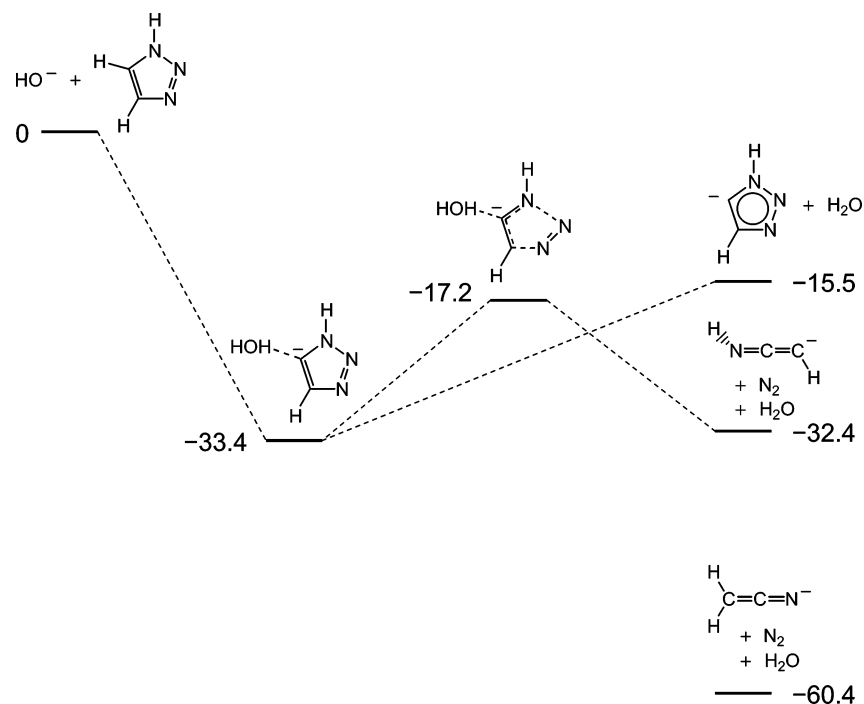


**Figure 3.** Energy diagram for the reaction of  $\text{HO}^-$  with  $1H$ -1,2,3-triazole to produce the ketenimine anion. The 298 K enthalpies are evaluated with B3LYP/6-311++G(d,p) calculations. The values represent the 298 K enthalpies of the intermediate and final product states relative to that of the reactant state in units of  $\text{kcal mol}^{-1}$ .

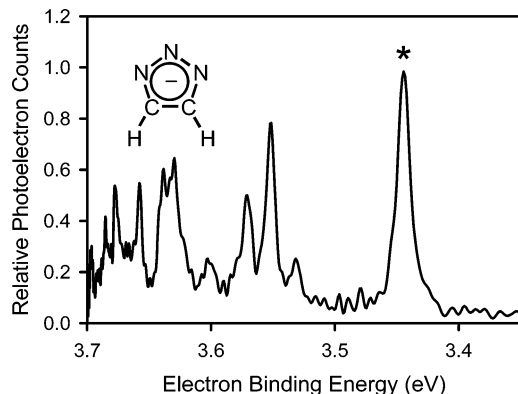


**Figure 4.** The 335 nm photoelectron-imaging spectrum of the 1,2,3-triazolide ion. The ions were synthesized through electron impact ionization of the pulsed supersonic expansion of an Ar gas mixture of  $\text{O}_2$ ,  $\text{CH}_4$ , and  $1H$ -1,2,3-triazole. The peak marked with an asterisk represents the vibrational origin of the electronic ground state of the 1,2,3-triazolyl radical.

supersonic expansion of the gas mixture (see Experimental Methods) produces secondary electrons that can dissociatively attach to  $\text{O}_2$  to form  $\text{O}^-$ . Then,  $\text{O}^-$  abstracts a H atom from  $\text{CH}_4$  to form  $\text{HO}^-$ , which subsequently deprotonates  $1H$ -1,2,3-triazole to generate  $m/z$  68 ions. If the deprotonation takes place at the N–H site, the  $m/z$  68 ions have the 1,2,3-triazolide structure.

B3LYP/6-311++G(d,p) calculations find a minimum for the potential energy surfaces of the 1,2,3-triazolide ion at  $C_{2v}$  symmetry. On the other hand, a minimum of the 1,2,3-triazolyl radical is found at  $C_s$  symmetry; the five-membered ring is not planar in the radical. The EA of the radical is calculated to be 3.477 eV. Thus, the peak marked with an asterisk in Figure 4 may be the vibrational origin of the electronic ground state of the radical. Spectral simulations have been performed with the *PESCAL* program,<sup>49,50</sup> using the optimized geometries and normal modes of the anion and radical ground states obtained from the DFT calculations. We have not been able to reproduce

the observed vibronic feature very well. While the same technique has been reasonably successful in the simulations of the photoelectron spectra of the pyrrolide<sup>8</sup> and imidazolid<sup>9</sup> ions, failure in the adiabatic simulation of the photoelectron spectrum of the pyrazolide ion has been attributed to the nonadiabatic coupling among the low-lying electronic states of the pyrazolyl radical.<sup>10,51</sup> We have recently demonstrated that the nonadiabatic effects on the vibronic structure of the low-lying states of the pyrazolyl radical can be successfully investigated using a diabatic model potential technique.<sup>51,52</sup> We have applied a similar technique and found large nonadiabatic interactions among the low-lying states of the 1,2,3-triazolyl radical. Details of the analysis of the nonadiabatic effects in the photoelectron spectrum will be described in a forthcoming paper.<sup>53</sup> However, this spectral analysis confirms that the peak marked with an asterisk in Figure 4 is the vibrational origin of the ground state of the 1,2,3-triazolyl radical. Thus, the EA of the radical is  $3.447 \pm 0.004$  eV.

This electron binding energy of the 1,2,3-triazolide ion is much larger than those of the azolide ions with two or fewer N atoms in the five-membered ring:  $1.812 \pm 0.005$  (cyclopentadienide),<sup>54</sup>  $2.145 \pm 0.010$  (pyrrolide),<sup>8</sup>  $2.613 \pm 0.006$  (imidazolid),<sup>9</sup> and  $2.938 \pm 0.005$  eV (pyrazolide).<sup>10</sup> An increase in the number of N atoms in the ring leads to an increase in the EA of the corresponding radical.

### 3. Photoelectron Spectrum of the Ketenimine Anion.

Figure 5 shows the 363.8 nm magic angle photoelectron spectrum of  $m/z$  40 ions produced from the reaction of  $\text{HO}^-$  with  $1H$ -1,2,3-triazole in the flowing afterglow ion source. The rather poor S/N ratio reflects a small ion beam current ( $\sim 10$  pA) obtained in the experiment. There are two broad bands apparent in the spectrum. The band in the lower eBE region is remeasured and displayed in Figure 6a. There are a few peaks noticeable in addition to the broad band. The peak at the lowest eBE corresponds to the origin peak of the photoelectron spectrum of the cyanomethyl anion. Another spectrum has been measured independently, as shown in Figure 6b, for the

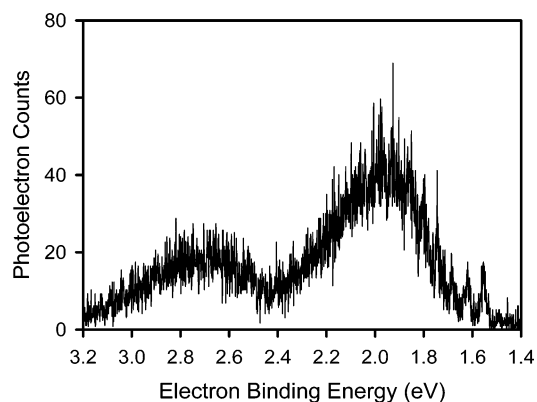


**Figure 5.** The 363.8 nm magic angle photoelectron spectrum of  $m/z$  40 ions produced from the reaction of  $\text{HO}^-$  with 1*H*-1,2,3-triazole in the flow tube at room temperature.

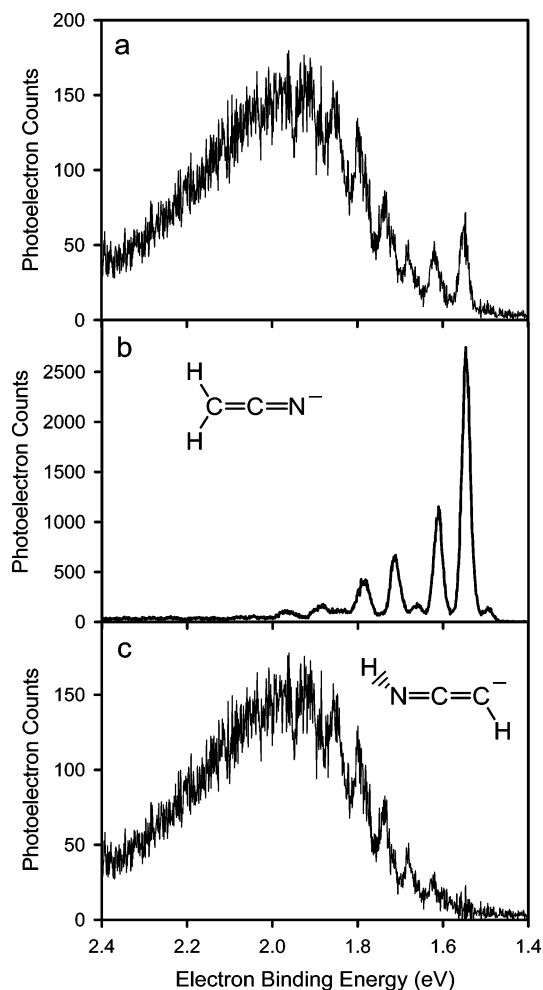


**Figure 6.** The 363.8 nm magic angle photoelectron spectra of (a)  $m/z$  40 ions produced from the reaction of  $\text{HO}^-$  with 1*H*-1,2,3-triazole in the flow tube at room temperature, and (b) the cyanomethyl anion produced from the reaction of  $\text{HO}^-$  with acetonitrile in the flow tube at room temperature. The spectrum in (b) is appropriately scaled and subtracted from the spectrum in (a), and the resultant spectrum is shown in (c).

cyanomethyl anion, which is produced from  $\text{HO}^-$  deprotonation of acetonitrile. This observed spectrum is consistent with a reported one,<sup>55</sup> but it has an improved resolution. The EA of the cyanomethyl radical is  $1.548 \pm 0.005$  eV. The spectrum in Figure 6c is the spectrum in Figure 6a less the contributions from the cyanomethyl anion. If the detachment cross sections

for the isomers were identical, then the cyanomethyl anion would account for only 5% of the total  $m/z$  40 population.<sup>56</sup>

We conclude that the spectrum shown in Figure 6c represents detachment from the electronic ground state of the ketenimine anion to that of the corresponding radical for the following reasons. The spectrum in Figure 6c exhibits a series of peaks that appear to be a vibrational progression with a frequency of  $465 \pm 30$   $\text{cm}^{-1}$ , which is reminiscent of the photoelectron spectrum of an isoelectronic ion, the allenyl anion.<sup>19,57</sup> An extensive vibrational progression for the out-of-plane CCH-bending mode of  $\tilde{X}^2B_1$  propargyl radical observed in the allenyl anion spectrum reflects a large geometry difference between the anion and radical states along that normal coordinate. The DFT calculations find a harmonic vibrational frequency of 491  $\text{cm}^{-1}$  for the out-of-plane CCH-bending mode of the  $^2A''$  ground state of the ketenimine radical. This calculated frequency is very close to the separations between the peaks in Figure 6c. While the potential energy minimum for the ground state of the ketenimine radical is located at  $C_s$  symmetry in the DFT calculations, that of the ketenimine anion has no symmetry with the H atom bonded to the terminal C atom displaced off the quasi-plane that the other four nuclei form. The CCH-bending angle is calculated to be  $129.0^\circ$  for the anion ground state. Thus, the appearance of the spectrum in Figure 6c is consistent with the optimized geometries and harmonic frequency evaluated in the DFT calculations. The DFT calculations predict the EA of the ketenimine radical to be 1.617 eV. The position of the smallest observable peak in the lowest eBE in Figure 6c is  $1.624 \pm 0.005$  eV. This eBE is very close to the calculated EA value. The large geometry difference along the CCH-bending coordinate between the anion and radical ground states is expected to diminish the Franck–Condon factor for the vibrational ground level of the radical ground state. Therefore, the calculated EA value is also consistent with our experimental observations. Actual determination of the EA value, however, needs careful analysis of the spectrum. A simulation of the spectrum is very difficult due to the anharmonic nature of the potential energy surfaces of the ketenimine anion as mentioned above. A detailed study of the spectral analysis is underway, and it will be reported in a future publication.<sup>58</sup> It should be noted that the broad band in the higher eBE region of the spectrum in Figure 5 represents detachment to the low-lying excited-state of the ketenimine radical.

The eBE of the ketenimine anion is much larger than that of the allenyl anion.<sup>19</sup> This increase can be ascribed to the presence of an N atom, analogous to the trend in the azolide series mentioned in the preceding section.

**4. Photoelectron Spectrum of the Iminodiazomethyl Anion.** We have positively identified the 1,2,3-triazolide ion in the photoelectron-imaging spectroscopic measurements as described in Section 2. Also, as presented in Section 3, the flowing afterglow-photoelectron spectroscopic measurements confirm the formation of the ketenimine anion in the reaction of  $\text{HO}^-$  with 1*H*-1,2,3-triazole. These results appear to fully explain the observations of  $m/z$  68 and  $m/z$  40 ions as the products in the FA-SIFT measurements detailed in Section 1. However, we have found that these two ions are not the only product ions of the reaction of  $\text{HO}^-$  with 1*H*-1,2,3-triazole.

Figure 7a shows the 363.8 nm magic angle photoelectron spectrum of  $m/z$  68 ions produced from the reaction of  $\text{HO}^-$  with 1*H*-1,2,3-triazole in the flowing afterglow ion source. It should be noted that the laser photon energy is not high enough to photodetach electrons from the 1,2,3-triazolide ion. A relatively intense spectral feature is seen in the eBE above 2.4

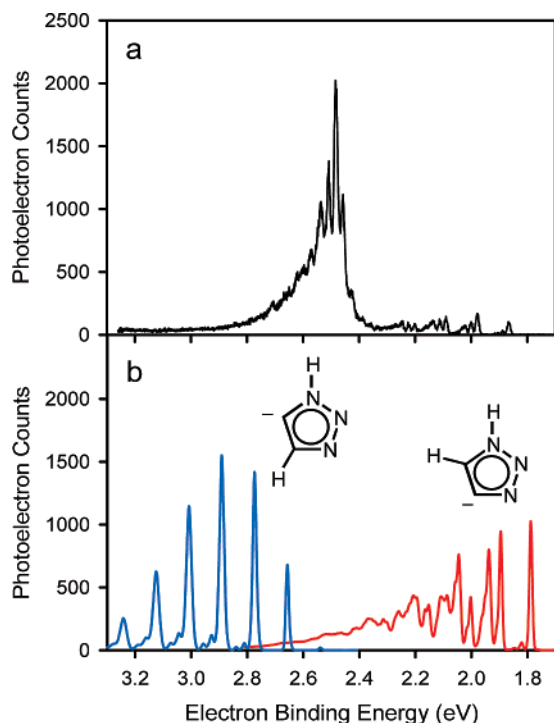


**Figure 7.** The 363.8 nm magic angle photoelectron spectrum of  $m/z$  68 ions produced from the reaction of  $\text{HO}^-$  with  $1H$ -1,2,3-triazole in the flow tube at room temperature (a). Simulations of the photoelectron spectra of the  $1H$ -1,2,3-triazol-4-ide (red) and  $1H$ -1,2,3-triazol-5-ide (blue) ions are shown in (b). The simulations are based on the optimized geometries, normal modes, and energetics of the electronic ground states of the anions and the corresponding radicals obtained from B3LYP/6-311++G(d,p) calculations.

eV with an anisotropy parameter,  $\beta$  (eq 1), of  $-0.3 \pm 0.1$ , while weak photoelectron signals are observed in the eBE below 2.4 eV.

We have confirmed the photoelectron spectrum of the 1,2,3-triazolide ion ( $m/z$  68) in Section 2, and the spectrum shown in Figure 7a cannot originate from the 1,2,3-triazolide ion. It is intuitive to suspect that  $m/z$  68 ions observed in Figure 7a arise from  $1H$ -1,2,3-triazole deprotonated at the C4–H and/or C5–H sites. B3LYP/6-311++G(d,p) calculations have been carried out to simulate the spectra of such ions. The simulated spectra of the  $1H$ -1,2,3-triazol-4-ide and  $1H$ -1,2,3-triazol-5-ide ions are shown in Figure 7b. The eBEs of the spectra are set to the DFT-calculated values. It is evident that neither spectral simulation can reproduce the observed features very well. Therefore, simple deprotonation of  $1H$ -1,2,3-triazole cannot account for these  $m/z$  68 ions. Nevertheless, the  $\text{HO}^-$  reaction with  $1H$ -1,2,3-triazole occurs most probably by proton transfer. We have already demonstrated how deprotonation at C5–H site leads to fragmentation of the ring structure as illustrated in Figure 3. Analogously, we explore possible chemical processes induced by deprotonation at the C4–H site through DFT calculations below.

An obvious isomerization process for the triazolide ion is ring-opening. Among possible bond fissions that would disrupt the ring structure following deprotonation of  $1H$ -1,2,3-triazole at the C4 position, a fission of the N1–N2 bond seems to be most likely because the resulting ion is the iminodiazomethyl anion (Figure 1). This ion is isoelectronic with the vinyl diazomethyl anion whose photoelectron spectrum has been measured in our recent study.<sup>59</sup>

Figure 8 summarizes the results of DFT calculations regarding the ring-opening process. Interaction of  $\text{HO}^-$  with  $1H$ -1,2,3-

triazole at the C4–H site can lead to formation of the ion–molecule complex stabilized relative to the reactants by 17.0 kcal mol<sup>-1</sup>. The energy barrier of N1–N2 bond fission for the isolated  $1H$ -1,2,3-triazol-4-ide ion is calculated to be 17.1 kcal mol<sup>-1</sup>. The energy level for the transition state shown in Figure 8 is evaluated by adding this energy barrier to the energy level of the ion–molecule complex. Once this barrier is overcome, four conformational isomers of the iminodiazomethyl anion can be generated. Two of them are depicted in Figure 8. The eBEs of these isomeric ions predicted by the DFT calculations (2.535 and 2.444 eV) are close to that for the most intense peak observed in Figure 7a.

We have simulated the photoelectron spectra of the different conformers of the iminodiazomethyl anion with the *PESCAL* program<sup>49,50</sup> based on the optimized geometries and normal modes of the anion and corresponding radical states obtained from the DFT calculations. The simulated spectrum for a mixture of the conformers successfully reproduces the higher eBE portion of the spectrum shown in Figure 7a. This spectral analysis supports the minor reaction pathway where  $\text{HO}^-$  deprotonates  $1H$ -1,2,3-triazole at the C4–H site to induce triazole ring-opening. Detailed analysis of the spectrum and discussion of the structure and energetics of the conformational isomers of the ring-opened ion will be given in a separate paper.<sup>60</sup>

### 5. Photoelectron Spectrum of the $2H$ -1,2,3-Triazol-4-ide Ion.

In the preceding sections, we have demonstrated that  $\text{HO}^-$  deprotonates  $1H$ -1,2,3-triazole at the N1–H site to form the 1,2,3-triazolide ion (Section 2), at the C5–H site to produce the ketenimine anion (Section 3), and at the C4–H site to generate the iminodiazomethyl anion (Section 4). The lower eBE portion of the photoelectron spectrum shown in Figure 7a, however, indicates presence of another  $m/z$  68 ion. We have already argued that  $1H$ -1,2,3-triazole-carbon-deprotonated ions, that is, the  $1H$ -1,2,3-triazol-4-ide and  $1H$ -1,2,3-triazol-5-ide ions, cannot account for this spectral feature (Figure 7b).

Another conceivable structural isomer is the  $2H$ -1,2,3-triazol-4-ide ion (Figure 1). We have carried out B3LYP/6-311++G(d,p) calculations for this ion and the corresponding radical. The EA of the  $2H$ -1,2,3-triazol-4-yl radical is calculated to be 1.879 eV. Figure 9a is a close-up of the lower eBE portion of the spectrum shown in Figure 7a. The DFT-calculated EA value is very close to the eBE of peak a. A spectral simulation has been performed for the transition from  $\tilde{X}^1A'$   $2H$ -1,2,3-triazol-4-ide ion to  $\tilde{X}^2A'$   $2H$ -1,2,3-triazol-4-yl radical based on the results of the DFT calculations. The DFT-optimized geometries of the anion and radical are given in Table 1. The simulated spectrum is shown in Figure 9b. The position of the origin peak of the simulation is set to that of peak a. The simulation reproduces the observed spectrum very well. Thus, the observed spectrum indicates that the  $2H$ -1,2,3-triazol-4-ide ion is produced in the flow tube.

Figure 10 illustrates the energy diagram for the reaction of  $\text{HO}^-$  with  $1H$ -1,2,3-triazole to produce the  $2H$ -1,2,3-triazol-4-ide ion. The DFT calculations suggest that deprotonation of  $1H$ -1,2,3-triazole at the N1–H site leads to formation of the 1,2,3-triazolide ion complexed with  $\text{H}_2\text{O}$  with about 62 kcal mol<sup>-1</sup> of excess energy. The site of  $\text{H}_2\text{O}$  complexation, that is, whether it is complexed at the N1 or N2 position, does not significantly change the energetics. It seems possible that  $\text{H}_2\text{O}$  reprotonates the 1,2,3-triazolide ion at the N2 position within the complex, and the regenerated  $\text{HO}^-$  deprotonates the newly formed  $2H$ -1,2,3-triazole at the C4–H site within the complex, generating

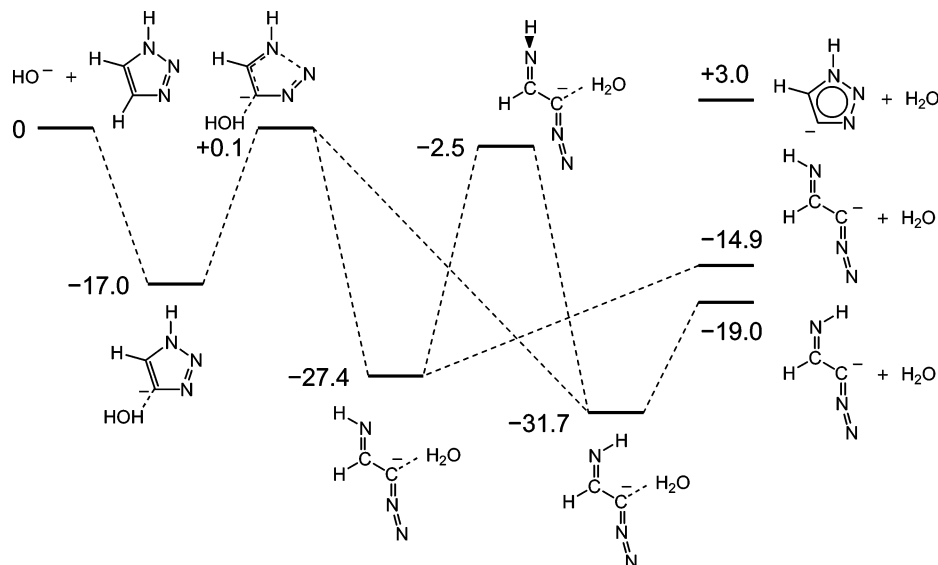


**Figure 8.** Energy diagram for the reaction of  $\text{HO}^-$  with 1*H*-1,2,3-triazole to produce the iminodiazomethyl anion. The 298 K enthalpies are evaluated with B3LYP/6-311++G(d,p) calculations. The values represent the 298 K enthalpies of the intermediate and final product states relative to that of the reactant state in units of  $\text{kcal mol}^{-1}$ .

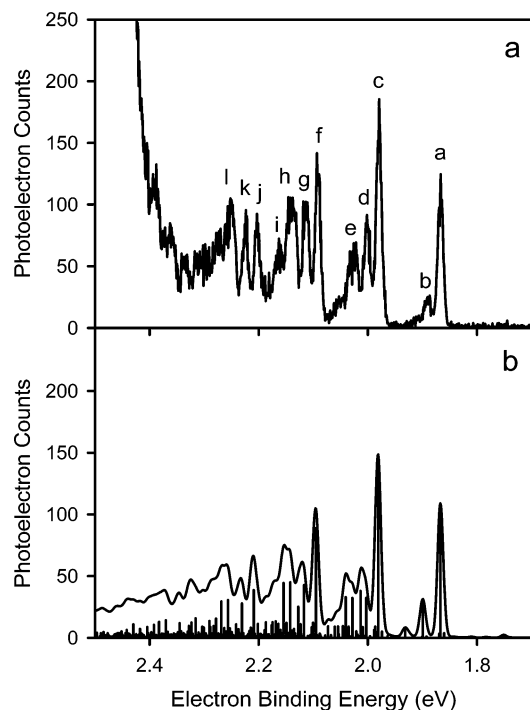


**Figure 9.** The 363.8 nm magic angle photoelectron spectrum of  $m/z$  68 ions produced from the reaction of  $\text{HO}^-$  with 1*H*-1,2,3-triazole in the flow tube at room temperature (a). A simulation of the photoelectron spectrum of the 2*H*-1,2,3-triazol-4-ide ion is shown in (b). Sticks represent relative positions and intensities of vibronic transitions from the  $\tilde{X}^1A'$  2*H*-1,2,3-triazol-4-ide ion to the  $\tilde{X}^2A'$  state of the corresponding radical. The solid line is a Gaussian convolution of the transitions with a full width at half-maximum of 12 meV. A vibrational temperature of 300 K was assumed for the anion in the simulation. The origin peak of the simulation is set to match peak a. The simulation is based on the optimized geometries and normal modes of the anion and the radical obtained from B3LYP/6-311++G(d,p) calculations.

the 2*H*-1,2,3-triazol-4-ide ion. The overall exothermicity is  $3.2 \text{ kcal mol}^{-1}$  according to the DFT calculations.

Following the successful simulation displayed in Figure 9b, the EA of the 2*H*-1,2,3-triazol-4-yl radical is determined to be  $1.865 \pm 0.004 \text{ eV}$ . A number of vibrational peaks observed in the spectrum are also identified through the spectral simulation.

**TABLE 1: B3LYP/6-311++G(d,p) Optimized Geometries for 2*H*-1,2,3-Triazol-4-ide Anion and 2*H*-1,2,3-Triazol-4-yl Radical<sup>a</sup>**

	$\tilde{X}^1A'$ anion	$\tilde{X}^2A'$ radical
N1N2	1.3328	1.3302
N2N3	1.3696	1.3379
N3C4	1.3565	1.3031
C4C5	1.4401	1.4054
C5N1	1.3402	1.3357
N2H	1.0089	1.0088
C5H	1.0837	1.0759
$\angle\text{N1N2N3}$	115.23	115.88
$\angle\text{N2N3C4}$	106.47	102.31
$\angle\text{N3C4C5}$	103.14	111.33
$\angle\text{C4C5N1}$	113.38	106.56
$\angle\text{C5N1N2}$	101.78	103.92
$\angle\text{N1N2H}$	121.40	121.91
$\angle\text{N1C5H}$	118.62	122.10

<sup>a</sup> Bond lengths are in units of angstroms, and bond angles are in units of degrees. See Figure 1 for the drawings of the molecular structures.

Peak b is a transition from the fundamental level of the N2–H out-of-plane bending mode of the anion ground state to that of the radical ground state. The DFT calculations find a very low harmonic frequency of  $231 \text{ cm}^{-1}$  for the bending mode of  $\tilde{X}^1A'$  2*H*-1,2,3-triazol-4-ide ion,<sup>61</sup> while the corresponding harmonic frequency is calculated to be  $491 \text{ cm}^{-1}$  for  $\tilde{X}^2A'$  2*H*-1,2,3-triazol-4-yl radical. Because the frequency for the out-of-plane mode of the final state is larger than that of the initial state, this hot band transition is expected to appear to the higher eBE side of the origin peak (peak a).<sup>62</sup> The position of peak b relative to peak a,  $185 \pm 25 \text{ cm}^{-1}$ , therefore, represents the difference in the fundamental frequency of the out-of-plane N2–H-bending mode between the anion and radical. Peak c is the fundamental level of the in-plane ring-bending mode centered at C4 with a frequency of  $910 \pm 10 \text{ cm}^{-1}$ . Peaks f and j represent a progression along this ring-bending mode. Peak d is composed mainly of two vibronic transitions. One is a transition to the fundamental level of an in-plane ring-stretching mode (N2–N3 and C4–C5), and the other is a combination of a transition to the fundamental of the C4-centered in-plane ring-bending mode and a hot band transition involving the out-of-plane N2–H-bending mode. Two other vibronic transitions

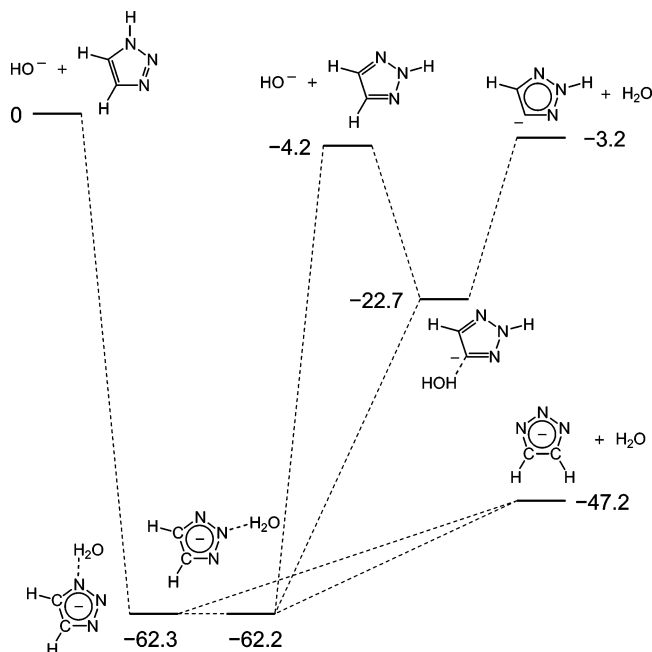


**Figure 10.** Energy diagram for the reaction of  $\text{HO}^-$  with  $1H$ -1,2,3-triazole to produce the  $2H$ -1,2,3-triazol-4-ide ion. The 298 K enthalpies are evaluated with B3LYP/6-311++G(d,p) calculations. The values represent the 298 K enthalpies of the intermediate and final product states relative to that of the reactant state in units of  $\text{kcal mol}^{-1}$ .

**TABLE 2: Peak Positions and Assignments for the Photoelectron Spectrum of  $2H$ -1,2,3-Triazol-4-ide Ion**

peak <sup>a</sup>	peak position ( $\text{cm}^{-1}$ ) <sup>b</sup>	assignment <sup>c</sup>
a	0	$0_0^0$
b	$185 \pm 25$	$15_1^1$
c	$910 \pm 10$	$11_0^1$
d	$1080 \pm 15$	$9_0^1$ and $11_0^1 15_1^1$
e	$1290 \pm 20$	$4_0^1$ and $6_0^1$
f	$1810 \pm 20$	$11_0^2$
g	$1985 \pm 20$	$9_0^1 11_0^1$ and $11_0^1 15_1^1$
h	$2190 \pm 30$	$4_0^1 11_0^1$ and $6_0^1 11_0^1$
i	$2395 \pm 50$	
j	$2710 \pm 30$	$11_0^3$
k	$2875 \pm 30$	$9_0^1 11_0^2$
l	$3115 \pm 30$	$4_0^1 11_0^2$ and $6_0^1 11_0^2$

<sup>a</sup> Peak labels used in Figure 9. <sup>b</sup>Relative to the origin peak (peak a). <sup>c</sup>The  $\nu_4$  mode is the (N1N2, N3C4) ring stretching,  $\nu_6$  is the (N1C5, N3C4) ring stretching,  $\nu_9$  is the (N2N3, C4C5) ring stretching, and  $\nu_{11}$  is the N3C4C5 ring-bending modes. All these modes are in-plane ( $a'$ ) modes. The  $\nu_{15}$  mode is the N2H out-of-plane bending mode.

account for peak e. These are transitions to the fundamental levels of two other in-plane ring-stretching modes; one involves N1–C5 and N3–C4 stretching, and the other entails N1–N2 and N3–C4 stretching. Positions and assignments of the observed peaks in Figure 9a are summarized in Table 2. Appearance of the peaks associated with these vibrational modes reflects considerable geometry differences along the corresponding normal coordinates, as shown in Table 1.

**6. The N–H BDE of  $2H$ -1,2,3-Triazole.** The EA of the 1,2,3-triazolyl radical determined in the present study (Section 2) can be combined with the gas-phase acidity of  $2H$ -1,2,3-triazole (see Section 1) to derive the N–H bond dissociation energy (BDE) of  $2H$ -1,2,3-triazole through a negative ion thermochemical cycle.<sup>63</sup>

$$D_0(2H\text{-}1,2,3\text{-triazole, N-H}) =$$

$$\Delta_{\text{acid}}H_0(2H\text{-}1,2,3\text{-triazole, N-H}) + \text{EA}(1,2,3\text{-triazolyl}) - \text{IE}(\text{H}) \quad (3)$$

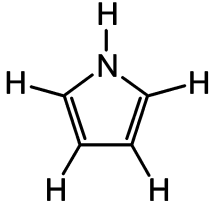
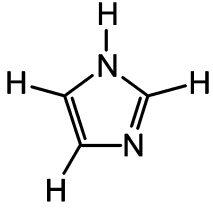
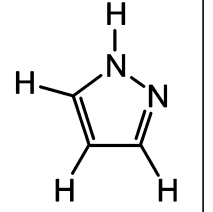
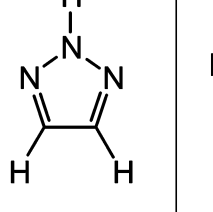
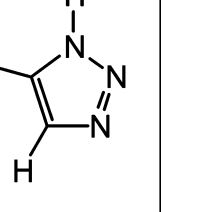
Here,  $\Delta_{\text{acid}}H_0$  is the 0 K N–H deprotonation enthalpy of  $2H$ -1,2,3-triazole, EA is the electron affinity of the 1,2,3-triazolyl radical, and IE(H) is the ionization energy of the H atom (13.59844 eV).<sup>64</sup> To obtain the 0 K N–H deprotonation enthalpy, the 298 K gas phase acidity of  $2H$ -1,2,3-triazole is first converted to the 298 K deprotonation enthalpy using the  $\Delta_{\text{acid}}S_{298}(2H\text{-}1,2,3\text{-triazole, N-H})$  value of  $25.6 \text{ cal mol}^{-1} \text{ K}^{-1}$  predicted by the DFT calculations:  $\Delta_{\text{acid}}H_{298}(2H\text{-}1,2,3\text{-triazole, N-H}) = 347.7 \pm 0.6 \text{ kcal mol}^{-1}$ . This 298 K deprotonation enthalpy is converted to the 0 K deprotonation enthalpy using the integrated heat capacities derived from the DFT calculations:  $\Delta_{\text{acid}}H_0(2H\text{-}1,2,3\text{-triazole, N-H}) = 346.3 \pm 0.6 \text{ kcal mol}^{-1}$ . This 0 K deprotonation enthalpy and the EA of the 1,2,3-triazolyl radical,  $3.447 \pm 0.004 \text{ eV}$ , are used in eq 3 to derive  $D_0(2H\text{-}1,2,3\text{-triazole, N-H}) = 112.2 \pm 0.6 \text{ kcal mol}^{-1}$ .

Our determination of the N2–H BDE of  $2H$ -1,2,3-triazole casts light on the effects of the N atoms in the five-membered, aromatic compounds on the N–H BDE. Ashfold and co-workers have used H Rydberg atom photofragment translational spectroscopy to quite accurately determine the N–H BDEs of pyrrole,<sup>65</sup>  $93.92 \pm 0.11 \text{ kcal mol}^{-1}$ , and imidazole,<sup>66,67</sup>  $95.04 \pm 0.11 \text{ kcal mol}^{-1}$ . We have previously determined the N–H BDEs of imidazole,<sup>9</sup>  $95.1 \pm 0.5 \text{ kcal mol}^{-1}$ , and pyrazole,<sup>10</sup>  $106.4 \pm 0.4 \text{ kcal mol}^{-1}$ , using negative ion thermochemical cycles. These results are summarized in Table 3.

Comparison of pyrrole and imidazole in Table 3 suggests that the presence of a  $\beta$ -aza substituent increases the N–H BDE only marginally, by  $1.1 \pm 0.2 \text{ kcal mol}^{-1}$ . On the other hand, a much larger increase in the N–H BDE by  $12.5 \pm 0.5 \text{ kcal mol}^{-1}$  arises due to the presence of an  $\alpha$ -aza substituent, as seen in comparison of pyrrole and pyrazole. The N–H BDE of  $2H$ -1,2,3-triazole, which possesses two  $\alpha$ -aza substituents, is even larger than that of pyrazole by  $5.8 \pm 0.8 \text{ kcal mol}^{-1}$ . It should also be pointed out that the  $1H$ -1,2,3-triazole is higher in energy than  $2H$ -1,2,3-triazole by  $4.2 \text{ kcal mol}^{-1}$  according to the DFT calculations.<sup>68</sup> Therefore, the N–H BDE of  $1H$ -1,2,3-triazole is expected to be about  $108 \text{ kcal mol}^{-1}$ . If this expected value is compared with the N–H BDE of pyrazole, then a  $\beta$ -aza substituent appears to affect the N–H BDE only slightly. Thus, the N–H BDE of  $2H$ -1,2,3-triazole determined in the present study establishes firmly a trend that an  $\alpha$ -aza substituent tends to increase the N–H BDE of azoles significantly.

The aza-substitution effects on the N–H BDE can be elucidated in terms of the negative ion thermochemical cycle (see eq 3). As one N atom replaces a C–H unit in the ring, the EA of the corresponding radical increases, which concomitantly increases the N–H BDE of the parent molecule according to the negative ion thermochemical cycle. The increases in the EA from pyrrolyl<sup>8</sup> to imidazolyl<sup>9</sup> and pyrazolyl<sup>10</sup> are  $0.468 \pm 0.012$  and  $0.793 \pm 0.012 \text{ eV}$ , respectively (Table 3). The effects of aza-substitution on the acidity of azoles at the N–H site have been discussed in the literature.<sup>69</sup> Aza-substitution at a  $\beta$ -position increases the N–H acidity more than that at an  $\alpha$ -position. Imidazole<sup>9</sup> is more acidic than pyrrole<sup>8</sup> by  $9.6 \pm 0.5 \text{ kcal mol}^{-1}$ , while pyrazole<sup>10</sup> is only  $5.8 \pm 0.6 \text{ kcal mol}^{-1}$  more acidic than pyrrole,<sup>8</sup> as seen in Table 3. The lowering of the gas-phase acidity value for imidazole is large enough to almost cancel the effect of the increase in EA on the N–H BDE of imidazole<sup>9</sup> on the right-hand side of the negative ion thermochemical cycle

TABLE 3: The N–H Bond Dissociation Energies, Electron Affinities, and Deprotonation Enthalpies for the Azole Systems<sup>a</sup>

					
	pyrrole	imidazole	pyrazole	2 <i>H</i> -1,2,3-triazole	1 <i>H</i> -1,2,3-triazole
$D_0$ (N–H) (kcal mol <sup>-1</sup> )	93.92 ± 0.11 <sup>b</sup>	95.04 ± 0.11 <sup>c</sup>	106.4 ± 0.4 <sup>d</sup>	112.2 ± 0.6 <sup>e</sup>	~108.0 <sup>f</sup>
EA (eV)	2.145 ± 0.010 <sup>g</sup>	2.613 ± 0.006 <sup>h</sup>	2.938 ± 0.005 <sup>d</sup>	3.447 ± 0.004 <sup>e</sup>	3.447 ± 0.004 <sup>e</sup>
$\Delta_{\text{acid}}H_0$ (N–H) (kcal mol <sup>-1</sup> )	358.0 ± 0.4 <sup>g</sup>	348.4 ± 0.2 <sup>i</sup>	352.2 ± 0.4 <sup>d</sup>	346.3 ± 0.6 <sup>j</sup>	~342.1 <sup>f</sup>

<sup>a</sup> The bond dissociation energies are for the N–H bonds of the azoles. The electron affinities are for the radicals produced by the N–H bond fission of the azoles. The 0 K deprotonation enthalpies are for the azoles at the N–H sites. <sup>b</sup>Ref 65. <sup>c</sup>Ref 67. <sup>d</sup>Ref 10. <sup>e</sup>Determined in the present study. <sup>f</sup>Derived from the corresponding value for 2*H*-1,2,3-triazole using the energy difference between the 1*H*- and 2*H*- isomers evaluated with B3LYP/6-311++G(d,p) calculations. <sup>g</sup>Ref 8. <sup>h</sup>Ref 9. <sup>i</sup>Derived from the N–H bond dissociation energy of imidazole (ref 67) and the electron affinity of the imidazolyl radical (ref 9) using a negative ion thermochemical cycle similar to eq 3. <sup>j</sup> $\Delta_{\text{acid}}G_{298}$  value from ref 43 is converted to  $\Delta_{\text{acid}}H_0$  value using the thermochemical values evaluated with B3LYP/6-311++G(d,p) calculations.

equation. On the other hand, pyrazole is not as acidic as imidazole, and combined with the larger EA increase the N–H BDE of pyrazole<sup>10</sup> is much larger than that of pyrrole.

The same argument applies to the triazole system. Because the same radical results from N–H bond fission of 1*H*-1,2,3-triazole and 2*H*-1,2,3-triazole, the amount of increase in the N–H BDE from pyrazole to the two triazoles due to the EA increase is the same. On the other hand, consistent with the general rule of the aza-substituent effects on the acidity of azoles,<sup>69</sup> 2*H*-1,2,3-triazole is more acidic than pyrazole only by 5.9 ± 0.8 kcal mol<sup>-1</sup>, while 1*H*-1,2,3-triazole is derived to be about 10 kcal mol<sup>-1</sup> more acidic than pyrazole using the results of the DFT calculations. The lowering of the acidity value is smaller for 2*H*-1,2,3-triazole, resulting in the larger N–H BDE. The decrease in the acidity value is large enough for 1*H*-1,2,3-triazole such that the N–H BDE of 1*H*-1,2,3-triazole is very close to that of pyrazole.<sup>10</sup>

This finding of the N atom effects on the N–H BDE of azoles is in stark contrast to those on the C–H BDE of azines, that is, six-membered, N-containing, aromatic molecules. It has been inferred in pyrolysis studies that the C–H BDEs of pyridine, pyrimidine, and pyrazine are significantly lowered when there is an  $\alpha$ -aza substituent.<sup>70–72</sup> This effect has been attributed to

stabilization of the radical formed by the C–H bond fission due to the interaction between an unpaired electron in the C-centered in-plane orbital and two unpaired electrons in the N-centered in-plane orbital of the radical.<sup>70–73</sup> Such a three-electron stabilization mechanism is absent for the radicals produced from the N–H bond fission of azoles, because the unpaired electron in the radical resides in an out-of-plane orbital, which is orthogonal to the N-centered in-plane orbital.<sup>8–10</sup>

**7. Ion Energetics for the HO<sup>-</sup> Reaction with 1*H*-1,2,3-Triazole.** In our previous study, HO<sup>-</sup> has been found to deprotonate pyrrole exclusively at the N–H site to produce the pyrrolide ion.<sup>8</sup> In HO<sup>-</sup> reactions with imidazole and pyrazole, however, we have observed formation of a minor amount of the C5–H deprotonated ions in the photoelectron spectroscopic measurements<sup>9,10</sup> in addition to N–H deprotonated ions, which are the major product ions. In the present study, four different product ion species have been identified experimentally, suggesting that initial HO<sup>-</sup> deprotonation of 1*H*-1,2,3-triazole occurs at all sites. Below, we comment on the energetics of these reaction processes schematically shown in Figures 2, 3, 8, and 10.

*7A. Deprotonation at the N1–H Site.* The major reaction pathway is the formation of the 1,2,3-triazolide ion, as illustrated

in Figure 2. The DFT calculations predict that this reaction is highly exothermic ( $47.2 \text{ kcal mol}^{-1}$ ). The large energy available for the ion–molecule complex ( $62.3 \text{ kcal mol}^{-1}$ ) can also facilitate other reaction processes (Figures 3, 8, and 10).

**7B. Deprotonation at the C5–H Site.** The DFT calculations suggest that the deprotonation enthalpy of 1*H*-1,2,3-triazole at the C5 position is  $373.7 \text{ kcal mol}^{-1}$ . This calculated value is much lower than those of pyrrole, imidazole, or pyrazole at the C5 position:  $396.0$ ,  $387.9$ , and  $384.4 \text{ kcal mol}^{-1}$ , respectively. These theoretical values can be compared with experimental values determined in our recent study<sup>11</sup> for *N*-methylimidazole and *N*-methylpyrazole;  $\Delta_{\text{acid}}H_{298}(\textit{N}\text{-methylimidazole, C5-H}) = 388.1 \pm 1.0 \text{ kcal mol}^{-1}$ , and  $\Delta_{\text{acid}}H_{298}(\textit{N}\text{-methylpyrazole, C5-H}) = 384.0 \pm 0.7 \text{ kcal mol}^{-1}$ . Imidazole and pyrazole are expected to be distinctly more acidic at the C5 position than pyrrole due to the  $\beta$ -aza substituent effects<sup>69</sup> (see also discussion in Section 6). There is a second  $\beta$ -aza substituent for the C5–H group in 1*H*-1,2,3-triazole, and the triazole is even more acidic at the C5 position. Although the reaction of  $\text{HO}^-$  with 1*H*-1,2,3-triazole to form the 1*H*-1,2,3-triazol-5-ide ion and  $\text{H}_2\text{O}$  is quite exothermic ( $\sim 15 \text{ kcal mol}^{-1}$ ) according to the DFT calculations (Figure 3), the 1*H*-1,2,3-triazol-5-ide ion has not been observed in our photoelectron spectroscopic measurements (see Figure 7) in contrast to the findings in the imidazolide<sup>9</sup> and pyrazolide<sup>10</sup> systems.

The absence of the 1*H*-1,2,3-triazol-5-ide ion may be justified if a more favorable reaction pathway exists following the deprotonation of 1*H*-1,2,3-triazole at the C5–H site. Indeed, the DFT calculations find a transition state for fragmentation of the isolated 1*H*-1,2,3-triazol-5-ide ion to the ketenimine anion and  $\text{N}_2$ , located  $16.2 \text{ kcal mol}^{-1}$  higher in energy than the ring-intact ion (Figure 3). It is true that this energy barrier can be perturbed significantly by interaction with  $\text{H}_2\text{O}$  within the ion–molecule complex. However, the calculated large  $\text{H}_2\text{O}$  complexation energy of  $33.4 \text{ kcal mol}^{-1}$  leads us to anticipate that this energy barrier can be overcome within the ion–molecule complex. It should also be mentioned that the entropy factor works in favor of the fragmentation pathway. Indeed, about one-third of the product ions from the reaction of  $\text{HO}^-$  with 1*H*-1,2,3-triazole are *m/z* 40 ions in the FA-SIFT experiments. We have confirmed the formation of the ketenimine anion in the photoelectron spectroscopic measurements (see Section 3 and Figure 6).<sup>74</sup>

When we use  $\text{O}^-$  as a reactant ion instead of  $\text{HO}^-$ , however, *m/z* 40 product ions are not observed in the reaction with 1*H*-1,2,3-triazole.  $\text{O}^-$  is a weaker base than  $\text{HO}^-$ :  $\Delta_{\text{acid}}H_{298}(\text{H}_2\text{O})^{39} = 390.27 \pm 0.03 \text{ kcal mol}^{-1}$ , and  $\Delta_{\text{acid}}H_{298}(\text{HO})^{75} = 382.60 \pm 0.07 \text{ kcal mol}^{-1}$ . This reduced exothermicity as well as the associated change in the energetics and chemistry of the ion–molecule complex prevent efficient formation of the ketenimine anion.

As mentioned in Section 1, similar fragmentation processes in solution initiated by the C5-ion structure have been reported in the literature<sup>45,46</sup> for the N1-substituted-1,2,3-triazole systems (see reaction 2). This generic fragmentation pattern has also been observed for the N1-substituted-tetrazole systems in solution.<sup>76–78</sup> To the best of our knowledge, our present study represents the first experimental observation of the ketenimine anion in the gas phase. Neutral ketenimine has been discussed in the context of astrochemistry,<sup>79</sup> and there have been several experimental studies reported in the literature.<sup>80–86</sup> It has also been reported that ketenimine is generated through pyrolysis of 1,2,3-triazole.<sup>83</sup> Recently, ketenimine has been detected toward the star-forming region Sagittarius B2(N).<sup>87</sup>

The fragmentation process for the 1*H*-1,2,3-triazol-5-ide ion can be compared with the  $\text{N}_2$  elimination through the ion chemistry of vinyl diazomethane that we have theoretically explored in our recent study.<sup>59</sup>  $\text{N}_2$  elimination takes place following deprotonation of vinyl diazomethane at the  $\beta$ -carbon. The energy barrier for this  $\text{N}_2$  elimination from the 1-diazomethylvinyl anion is only  $2.3 \text{ kcal mol}^{-1}$  according to the DFT calculations. Similar to the vinyl diazomethane system,  $\text{N}_2$  elimination from 1*H*-1,2,3-triazole is facilitated by deprotonation at the  $\beta$ -carbon with respect to the dissociating  $\text{N}_2$ . Nevertheless, the calculated energy barrier,  $16.2 \text{ kcal mol}^{-1}$ , is much higher than that for the vinyl diazomethane system. Such a high-energy barrier may reflect the rather stable ring structure of the 1*H*-1,2,3-triazol-5-ide ion, which has two  $\beta$ -aza substituents as well as an adjacent N–H group.

The 1*H*-1,2,3-triazol-5-ide ion is isoelectronic with the pentazolide ion ( $\text{N}_5^-$ ), and its fragmentation to the ketenimine anion and  $\text{N}_2$  parallels the fragmentation of  $\text{N}_5^-$  to  $\text{N}_3^-$  and  $\text{N}_2$ .<sup>88</sup> The energy barrier and exothermicity of the fragmentation of the 1*H*-1,2,3-triazol-5-ide ion are  $16.2$  and  $19.0 \text{ kcal mol}^{-1}$ , respectively, according to the DFT calculations. The corresponding values for the fragmentation of  $\text{N}_5^-$  are predicted to be  $27.7$  and  $14 \text{ kcal mol}^{-1}$ , respectively.<sup>89</sup> It should be noted, however, that the ketenimine anion is not the most stable isomer, located  $28.0 \text{ kcal mol}^{-1}$  higher in energy than the cyanomethyl anion (see Figure 3).

**7C. Deprotonation of C4–H Site.** Deprotonation of 1*H*-1,2,3-triazole at the C4 position is not energetically favorable because the C4–H site is not adjacent to the N–H group, although there is one  $\beta$ -aza substituent.<sup>69</sup> The DFT calculations predict a deprotonation enthalpy of  $392.2 \text{ kcal mol}^{-1}$  for the C4–H site, suggesting that  $\text{HO}^-$  deprotonation of 1*H*-1,2,3-triazole at the C4 position is slightly endothermic (Figure 8). Indeed, our photoelectron spectra show no sign of the 1*H*-1,2,3-triazol-4-ide ion (Figure 7). Instead, we have observed the photoelectron spectrum of the ring-opened iminodiazomethyl anion (Figure 7a). The only plausible pathway for the formation of this ion involves  $\text{HO}^-$  deprotonation of 1*H*-1,2,3-triazole at the C4–H site, as illustrated in Figure 8. According to the DFT calculations, N1–N2 bond fission takes place from the isolated 1*H*-1,2,3-triazol-4-ide ion with an energy barrier of  $17.1 \text{ kcal mol}^{-1}$ . This energy is comparable to the association energy available for the ion–molecule complex. Good photoelectron signals for photodetachment from the iminodiazomethyl anion suggest that the energy barrier for the N1–N2 bond fission within the ion–molecule complex is significantly lowered.

It should be noted that when  $\text{O}^-$  is used as a reactant ion instead of  $\text{HO}^-$  the photoelectron spectrum of the iminodiazomethyl anion is not observed in the reaction with 1*H*-1,2,3-triazole, even though the beam current of *m/z* 68 ion is comparable to that obtained from the  $\text{HO}^-$  reaction (cf. discussion in Section 7B regarding the  $\text{O}^-$  reaction). This observation suggests that  $\text{O}^-$  is not sufficiently basic to drive the ring-opening process, and the reaction of  $\text{O}^-$  with 1*H*-1,2,3-triazole can produce only the 1,2,3-triazolide ion through deprotonation at the N1–H site.

The ion chemistry of 1*H*-1,2,3-triazole is compared with that of vinyl diazomethane (see also discussion in Section 7B). As described in our recent study,<sup>59</sup> the reaction of the allyl anion with  $\text{N}_2\text{O}$  is expected to proceed through an intermediate  $\text{HO}^-$ –vinyl diazomethane complex. The relative yields of the product ions reflect the difference in the acidities of vinyl diazomethane at the  $\alpha$ - and  $\beta$ -carbon atoms. Because vinyl diazomethane is most acidic at the  $\text{C}_\alpha$  atom, the major product ions are

vinylidiazomethyl anions. A minor fraction of the product ions is the allenyl anion ( $+N_2$ ), resulting from deprotonation of vinylidiazomethane at the  $C_\beta$  atom followed by  $N_2$  dissociation.

The relative acidities for the 1*H*-1,2,3-triazole sites are opposite to those for vinylidiazomethane. As mentioned earlier, the DFT calculations suggest that 1*H*-1,2,3-triazole is much more acidic at the C5 position than at the C4 position. The C5–H site is adjacent to the N–H group and has two  $\beta$ -aza substituents. It has also been reported that lithiation of N-substituted-1,2,3-triazole is much more facile at the C5 position in solution.<sup>45</sup> This acidity difference favors formation of the ketenimine anion, which is isoelectronic with the allenyl anion, over that of the iminodiazomethyl anion, which is isoelectronic with the vinylidiazomethyl anion. Of course, the relative yields also depend on the intrinsic energy barriers for the fragmentation and ring-opening. As seen in Figures 3 and 8, the overall energy barrier for formation of the ketenimine anion is much lower than that of the iminodiazomethyl anion due to the difference in ion–molecule complexation energy, which reflects the relative acidities. Indeed, our results of FA-SIFT measurements (Section 1) support the idea that the ketenimine anion is more abundant than the iminodiazomethyl anion because most of the  $m/z$  68 ions have been identified as 1,2,3-triazolide ions.<sup>74</sup>

**7D. The  $HO^-$ -Mediated Proton Migration from the N1 to N2 Positions.** The DFT calculations predict that the deprotonation enthalpy of 2*H*-1,2,3-triazole at the C4 position is 390.2 kcal mol<sup>-1</sup>. Thus, the proton-transfer reaction of  $HO^-$  with 2*H*-1,2,3-triazole at the C4–H site is almost thermoneutral ( $\Delta_{acid}H_{298}(H_2O)^{39} = 390.27 \pm 0.03$  kcal mol<sup>-1</sup>; see also Figure 10). In the presence of the highly acidic N2–H site ( $\Delta_{acid}H_{298}(2H-1,2,3-triazole, N-H) = 347.7 \pm 0.6$  kcal mol<sup>-1</sup>; see Section 1), C4–H deprotonation would be largely suppressed in the direct reaction of  $HO^-$  with 2*H*-1,2,3-triazole. On the other hand, 1*H*-1,2,3-triazole is 4.2 kcal mol<sup>-1</sup> higher in energy than 2*H*-1,2,3-triazole according to the DFT calculations. Thus, the  $HO^-$  reaction of 1*H*-1,2,3-triazole leading to the formation of the 2*H*-1,2,3-triazol-4-ide ion, as shown in Figure 10, is slightly exothermic. It should be noted that the reaction of  $O^-$  with 1*H*-1,2,3-triazole to form the 2*H*-1,2,3-triazol-4-ide ion is endothermic. Indeed, the 2*H*-1,2,3-triazol-4-ide ion has not been detected through photoelectron spectroscopic measurements when  $O^-$  is used as the reactant ion.

We cannot rule out the possibility that the 2*H*-1,2,3-triazol-4-ide ion is formed by the reaction of  $HO^-$  with 2*H*-1,2,3-triazole, which may be present in a significant amount in the flow tube. A microwave study found that 1,2,3-triazole was predominantly in the 2*H*-tautomeric form in the gas phase.<sup>44</sup> On the other hand, the triazole is predominantly in the 1*H*-tautomeric form in the liquid sample used in our experiments. It is uncertain how thermal equilibration between the 1*H*- and 2*H*-forms is achieved as the molecules are introduced into the flow tube. The ion source conditions in our experiments are such that the residence time of the reactants is on the order of 10 ms. This condition is drastically different from that used in the microwave study where the cell was saturated with 1,2,3-triazole over a period of several days before measurements.<sup>44</sup> Indeed, formation of the ketenimine anion and the iminodiazomethyl anion with significant yields suggests that the 1*H*-tautomer must be present in a considerable abundance. In light of the energetic considerations described in the preceding paragraph, we propose that the reaction of  $HO^-$  with 1*H*-1,2,3-triazole produces the majority of the 2*H*-1,2,3-triazol-4-ide ions observed in our measurements.

We have not observed the photoelectron spectra of the 1*H*-1,2,3-triazol-4-ide ion or the 1*H*-1,2,3-triazol-5-ide ion (Figure 7). As explained earlier,  $HO^-$  deprotonation of 1*H*-1,2,3-triazole at the C4–H and C5–H sites leads to ring-opening and fragmentation, respectively. According to the DFT calculations, the complex of the 2*H*-1,2,3-triazol-4-ide ion with  $H_2O$  is stabilized by 22.7 kcal mol<sup>-1</sup> relative to the initial reactants; that is,  $HO^-$  and 1*H*-1,2,3-triazole (Figure 10). While this complexation energy is not as large as that for the complex of the 1*H*-1,2,3-triazol-5-ide ion with  $H_2O$  (Figure 3), it is greater than that for the complex of the 1*H*-1,2,3-triazol-4-ide ion with  $H_2O$  (Figure 8). The fact that the 2*H*-1,2,3-triazol-4-ide ion has been observed in the photoelectron spectroscopic measurements may indicate that the ion is rather stable with respect to fragmentation or ring-opening. Thus, it seems that the position of the N–H site in the triazolide ions influences the stability of the ring structure significantly.

## Conclusions

The reaction of  $HO^-$  with 1*H*-1,2,3-triazole has been studied experimentally using an FA-SIFT technique, photoelectron-imaging spectroscopy, and flowing afterglow-photoelectron spectroscopy. B3LYP/6-311++G(d,p) calculations have been performed to explain the reaction mechanism leading to formation of the product ions observed in the experiments. In FA-SIFT measurements, major product ions are  $m/z$  68 ions while a significant fraction of the product ions corresponds to  $m/z$  40 ions. The photoelectron-imaging spectrum of the 1,2,3-triazolide ion has been measured, confirming the major product  $m/z$  68 ion of the reaction, produced by deprotonation of the triazole at the N1–H site. The EA of the 1,2,3-triazolyl radical is determined to be  $3.447 \pm 0.004$  eV. The EA of the 1,2,3-triazolyl radical and the gas-phase acidity of 2*H*-1,2,3-triazole are utilized in a negative ion thermochemical cycle to determine the N–H BDE of 2*H*-1,2,3-triazole to be  $112.2 \pm 0.6$  kcal mol<sup>-1</sup>. The photoelectron spectrum of the ketenimine anion has also been measured. The  $HO^-$  deprotonation of 1*H*-1,2,3-triazole at the C5–H site is followed by triazole ring fragmentation to produce this  $m/z$  40 ion and  $N_2$ . Formation of the iminodiazomethyl anion ( $m/z$  68) has also been confirmed in photoelectron spectroscopic measurements.  $HO^-$  deprotonates 1*H*-1,2,3-triazole at the C4–H site, and the ensuing N1–N2 bond fission yields this ring-opened iminodiazomethyl anion. The photoelectron spectrum of the 2*H*-1,2,3-triazol-4-ide ion ( $m/z$  68) has also been observed. Following the  $HO^-$  deprotonation of 1*H*-1,2,3-triazole at the N1–H site, the 1,2,3-triazolide ion is reprotonated by  $H_2O$  at the N2 position within the ion–molecule complex, and the newly formed 2*H*-1,2,3-triazole is again deprotonated by  $HO^-$  at the C4–H site within the same complex to produce the 2*H*-1,2,3-triazol-4-ide ion. The EA of the 2*H*-1,2,3-triazol-4-yl radical is  $1.865 \pm 0.004$  eV.

The present study, combining multiple experimental techniques and electronic structure calculations, reveals the complexity of the ion chemistry of 1*H*-1,2,3-triazole and the ion energetics of the five-membered ring system containing three N atoms. Comparison with our previous studies of the azoles with fewer N atoms clearly demonstrates the effects of an additional N atom on the chemistry and thermodynamic properties of the nitrogen-rich compound.

**Acknowledgment.** We are grateful to Professor John F. Stanton for his help in understanding the nonadiabatic effects in the photoelectron spectrum of the 1,2,3-triazolide ion. We would like to thank Dr. Richard K. Shoemaker for examining

the purity of the triazole sample by NMR. We are pleased to acknowledge generous support from the Air Force Office of Scientific Research and the National Science Foundation. We are pleased to dedicate this paper to Casey Hynes, an incomparable scholar, superb scientist, and dear friend.

## References and Notes

- (1) Klapotke, T. M. *Angew. Chem., Int. Ed.* **1999**, *38*, 2536–2538.
- (2) Nguyen, M. T. *Coord. Chem. Rev.* **2003**, *244*, 93–113.
- (3) Kwon, O.; McKee, M. L. Polynitrogens as promising high-energy density materials: computational design. In *Energetic Materials, Part 1: Decomposition, Crystal and Molecular Properties*; Politzer, P., Murray, J. S., Eds.; Elsevier: Amsterdam, 2003; pp 405–420.
- (4) Brinck, T.; Bittererova, M.; Ostmark, H. Electronic structure calculations as a tool in the quest for experimental verification of N<sub>4</sub>. In *Energetic Materials, Part 1: Decomposition, Crystal and Molecular Properties*; Politzer, P., Murray, J. S., Eds.; Elsevier: Amsterdam, 2003; pp 421–439.
- (5) Fau, S.; Bartlett, R. J. Changing the properties of N<sub>5</sub><sup>+</sup> and N<sub>5</sub><sup>-</sup> by substitution. In *Energetic Materials, Part 1: Decomposition, Crystal and Molecular Properties*; Politzer, P., Murray, J. S., Eds.; Elsevier: Amsterdam, 2003; pp 441–455.
- (6) Singh, R. P.; Verma, R. D.; Meshri, D. T.; Shreeve, J. M. *Angew. Chem., Int. Ed.* **2006**, *45*, 3584–3601.
- (7) Samartzis, P. C.; Wodtke, A. M. *Int. Rev. Phys. Chem.* **2006**, *25*, 527–552.
- (8) Gianola, A. J.; Ichino, T.; Hoeningman, R. L.; Kato, S.; Bierbaum, V. M.; Lineberger, W. C. *J. Phys. Chem. A* **2004**, *108*, 10326–10335.
- (9) Gianola, A. J.; Ichino, T.; Hoeningman, R. L.; Kato, S.; Bierbaum, V. M.; Lineberger, W. C. *J. Phys. Chem. A* **2005**, *109*, 11504–11514.
- (10) Gianola, A. J.; Ichino, T.; Kato, S.; Bierbaum, V. M.; Lineberger, W. C. *J. Phys. Chem. A* **2006**, *110*, 8457–8466.
- (11) Villano, S. M.; Gianola, A. J.; Eyet, N.; Ichino, T.; Kato, S.; Bierbaum, V. M.; Lineberger, W. C. *J. Phys. Chem. A* **2007**, *111*, 8579–8587.
- (12) DePuy, C. H. *Org. Mass Spectrom.* **1985**, *20*, 556–559.
- (13) Bierbaum, V. M.; Grabowski, J. J.; DePuy, C. H. *J. Phys. Chem.* **1984**, *88*, 1389–1393.
- (14) Kass, S. R.; Filley, J.; Van Doren, J. M.; DePuy, C. H. *J. Am. Chem. Soc.* **1986**, *108*, 2849–2852.
- (15) DePuy, C. H.; Barlow, S. E.; Van Doren, J. M.; Roberts, C. R.; Bierbaum, V. M. *J. Am. Chem. Soc.* **1987**, *109*, 4414–4415.
- (16) Chou, P. K.; Kass, S. R. *J. Am. Chem. Soc.* **1991**, *113*, 4357–4359.
- (17) O'Hair, R. A. J.; Gronert, S.; DePuy, C. H. *Eur. Mass Spectrom.* **1995**, *1*, 429–436.
- (18) DePuy, C. H.; Bierbaum, V. M.; Robinson, M. S.; Davico, G. E.; Gareyev, R. *Tetrahedron* **1997**, *53*, 9847–9856.
- (19) Robinson, M. S.; Polak, M. L.; Bierbaum, V. M.; DePuy, C. H.; Lineberger, W. C. *J. Am. Chem. Soc.* **1995**, *117*, 6766–6778.
- (20) Gunion, R. F.; Karney, W.; Wenthold, P. G.; Borden, W. T.; Lineberger, W. C. *J. Am. Chem. Soc.* **1996**, *118*, 5074–5082.
- (21) Wenthold, P. G.; Squires, R. R.; Lineberger, W. C. *J. Am. Chem. Soc.* **1998**, *120*, 5279–5290.
- (22) Nimlos, M. R.; Davico, G.; Geise, C. M.; Wenthold, P. G.; Lineberger, W. C.; Blanksby, S. J.; Hadad, C. M.; Petersson, G. A.; Ellison, G. B. *J. Chem. Phys.* **2002**, *117*, 4323–4339.
- (23) Van Doren, J. M.; Barlow, S. E.; DePuy, C. H.; Bierbaum, V. M. *Int. J. Mass Spectrom. Ion Processes* **1987**, *81*, 85–100.
- (24) Bierbaum, V. M. Flow Tubes. In *Encyclopedia of Mass Spectrometry*; Gross, M. L., Caprioli, R., Eds.; Elsevier: Amsterdam, 2003; Vol. 1, pp 276–292.
- (25) Rathbone, G. J.; Sanford, T.; Andrews, D.; Lineberger, W. C. *Chem. Phys. Lett.* **2005**, *401*, 570–574.
- (26) Sanford, T.; Han, S. Y.; Thompson, M. A.; Parson, R.; Lineberger, W. C. *J. Chem. Phys.* **2005**, *122*, 054307.
- (27) Dribinski, V.; Ossadtchi, A.; Mandelshtam, V. A.; Reisler, H. *Rev. Sci. Instrum.* **2002**, *73*, 2634–2642.
- (28) Cooper, J.; Zare, R. N. *J. Chem. Phys.* **1968**, *48*, 942–943.
- (29) Andersen, T.; Haugen, H. K.; Hotop, H. *J. Phys. Chem. Ref. Data* **1999**, *28*, 1511–1533.
- (30) Rienstra-Kiracofe, J. C.; Tschumper, G. S.; Schaefer, H. F.; Nandi, S.; Ellison, G. B. *Chem. Rev.* **2002**, *102*, 231–282.
- (31) Leopold, D. G.; Murray, K. K.; Stevens, Miller, A. E.; Lineberger, W. C. *J. Chem. Phys.* **1985**, *83*, 4849–4865.
- (32) Ervin, K. M.; Ho, J.; Lineberger, W. C. *J. Chem. Phys.* **1989**, *91*, 5974–5992.
- (33) Ervin, K. M.; Lineberger, W. C. Photoelectron Spectroscopy of Negative Ions. In *Advances in Gas Phase Ion Chemistry*; Adams, N. G., Babcock, L. M., Eds.; JAI Press: Greenwich, 1992; Vol. 1, pp 121–166.
- (34) Frisch, M. J.; Trucks, G. W.; Schlegel, H. B.; Scuseria, G. E.; Robb, M. A.; Cheeseman, J. R.; Montgomery, J. A., Jr.; Vreven, T.; Kudin, K. N.; Burant, J. C.; Millam, J. M.; Iyengar, S. S.; Tomasi, J.; Barone, V.; Mennucci, B.; Cossi, M.; Scalmani, G.; Rega, N.; Petersson, G. A.; Nakatsuji, H.; Hada, M.; Ehara, M.; Toyota, K.; Fukuda, R.; Hasegawa, J.; Ishida, M.; Nakajima, T.; Honda, Y.; Kitao, O.; Nakai, H.; Klene, M.; Li, X.; Knox, J. E.; Hratchian, H. P.; Cross, J. B.; Bakken, V.; Adamo, C.; Jaramillo, J.; Gomperts, R.; Stratmann, R. E.; Yazyev, O.; Austin, A. J.; Cammi, R.; Pomelli, C.; Ochterski, J. W.; Ayala, P. Y.; Morokuma, K.; Voth, G. A.; Salvador, P.; Dannenberg, J. J.; Zakrzewski, V. G.; Dapprich, S.; Daniels, A. D.; Strain, M. C.; Farkas, O.; Malick, D. K.; Rabuck, A. D.; Raghavachari, K.; Foresman, J. B.; Ortiz, J. V.; Cui, Q.; Baboul, A. G.; Clifford, S.; Cioslowski, J.; Stefanov, B. B.; Liu, G.; Liashenko, A.; Piskorz, P.; Komaromi, I.; Martin, R. L.; Fox, D. J.; Keith, T.; Al-Laham, M. A.; Peng, C. Y.; Nanayakkara, A.; Challacombe, M.; Gill, P. M. W.; Johnson, B.; Chen, W.; Wong, M. W.; Gonzalez, C.; Pople, J. A. *Gaussian 03*, Revision B.05; Gaussian, Inc.: Wallingford, CT, 2004.
- (35) Becke, A. D. *J. Chem. Phys.* **1993**, *98*, 5648–5652.
- (36) Lee, C. T.; Yang, W. T.; Parr, R. G. *Phys. Rev. B* **1988**, *37*, 785–789.
- (37) Krishnan, R.; Binkley, J. S.; Seeger, R.; Pople, J. A. *J. Chem. Phys.* **1980**, *72*, 650–654.
- (38) Shiell, R. C.; Hu, X. K.; Hu, Q. J.; Hepburn, J. W. *J. Phys. Chem. A* **2000**, *104*, 4339–4342.
- (39) Ervin, K. M.; DeTuro, V. F. *J. Phys. Chem. A* **2002**, *106*, 9947–9956.
- (40) Cumming, J. B.; Kebarle, P. *Can. J. Chem.* **1978**, *56*, 1–9.
- (41) Martin, J. D. D.; Hepburn, J. W. *J. Chem. Phys.* **1998**, *109*, 8139–8142.
- (42) The gas-phase acidity of HCOOH has been derived from the results of the proton transfer equilibrium measurements between HCOOH and HCl (ref 40) and a precise measurement of the gas-phase acidity of HCl (ref 41).
- (43) Catalan, J.; Claramunt, R. M.; Elguero, J.; Laynez, J.; Menendez, M.; Anvia, F.; Quian, J. H.; Taagepera, M.; Taft, R. W. *J. Am. Chem. Soc.* **1988**, *110*, 4105–4111.
- (44) Begtrup, M.; Nielsen, C. J.; Nygaard, L.; Samdal, S.; Sjogren, C. E.; Sorensen, G. O. *Acta Chem. Scand., Ser. A* **1988**, *42*, 500–514.
- (45) Raap, R. *Can. J. Chem.* **1971**, *49*, 1792–1798.
- (46) Ghose, S.; Gilchrist, T. L. *J. Chem. Soc., Perkin Trans. 1* **1991**, 775–779.
- (47) The B3LYP/6–311++G(d,p) energy optimization has been performed under C<sub>s</sub> symmetry for the H<sub>2</sub>O complex. A low imaginary frequency has been found in the harmonic frequency analysis at the stationary point with respect to hindered rotation around the OH bond. Thus, the potential energy minimum is located at C<sub>1</sub> symmetry, but energy lowering from the C<sub>s</sub> to C<sub>1</sub> geometry is 0.1 kcal mol<sup>-1</sup> or less in magnitude. The reported value is that for the C<sub>s</sub> symmetry.
- (48) A saddle point has been located under C<sub>s</sub> symmetry. Two imaginary frequencies have been found at the stationary point. One mode involves N1–N2 and N3–C4 stretching, which represents the N<sub>2</sub> dissociation coordinate. The other mode is an out-of-plane mode that guides the C<sub>2</sub>H<sub>2</sub>N ion fragment into the optimum geometry of the ketenimine anion. The reported energy barrier is for this saddle point, and the energy barrier for the actual transition state may be slightly lower.
- (49) Ervin, K. M.; Ramond, T. M.; Davico, G. E.; Schwartz, R. L.; Casey, S. M.; Lineberger, W. C. *J. Phys. Chem. A* **2001**, *105*, 10822–10831.
- (50) Ervin, K. M. *PESCAL*, Fortran Program; University of Nevada, Reno, NV, 2003.
- (51) Ichino, T.; Gianola, A. J.; Lineberger, W. C.; Stanton, J. F. *J. Chem. Phys.* **2006**, *125*, 084312.
- (52) Köppel, H.; Domcke, W.; Cederbaum, L. S. *Adv. Chem. Phys.* **1984**, *57*, 59–246.
- (53) Ichino, T.; Andrews, D. H.; Rathbone, G. J.; Misaizu, F.; Calvi, R. M. D.; Lineberger, W. C.; Stanton, J. F., to be published.
- (54) Ichino, T.; Rathbone, G. J.; Wren, S. W.; Gianola, A. J.; Lineberger, W. C.; Stanton, J. F. University of Colorado, Boulder, CO. To be submitted for publication.
- (55) Moran, S.; Ellis, Jr., H. B.; DeFrees, D. J.; McLean, A. D.; Ellison, G. B. *J. Am. Chem. Soc.* **1987**, *109*, 5996–6003.
- (56) It is unclear whether the cyanomethyl anion observed in the photoelectron spectrum (Figure 6a) results from the ion chemistry involving 1H-1,2,3-triazole or from some impurity reactions in the flow tube. However, the acetonitrile impurity in the triazole sample is <0.1% according to NMR measurements.
- (57) Oakes, J. M.; Ellison, G. B. *J. Am. Chem. Soc.* **1983**, *105*, 2969–2975.
- (58) Ichino, T.; Wren, S. W.; Lineberger, W. C.; Stanton, J. F. University of Colorado, Boulder, CO. To be submitted for publication.
- (59) Ichino, T.; Gianola, A. J.; Kato, S.; Bierbaum, V. M.; Lineberger, W. C. *J. Phys. Chem. A* **2007**, *111*, 8374–8383.

(60) Ichino, T.; Wren, S. W.; Andrews, D. H.; Kato, S.; Bierbaum, V. M.; Lineberger, W. C. University of Colorado, Boulder, CO. To be submitted for publication.

(61) B3LYP/6-311++G(d,p) calculations find low harmonic frequencies for the N-H out-of-plane bending modes of the C4-deprotonated azolide ions in general.

(62) A transition from this vibrationally excited level of the anion ground state to the vibrational ground level of the radical ground state is symmetry forbidden.

(63) Berkowitz, J.; Ellison, G. B.; Gutman, D. *J. Phys. Chem.* **1994**, *98*, 2744–2765.

(64) NIST Standard Reference Database Number 69, June 2005 Release.

(65) Cronin, B.; Nix, M. G. D.; Qadiri, R. H.; Ashfold, M. N. R. *Phys. Chem. Chem. Phys.* **2004**, *6*, 5031–5041.

(66) Ashfold, M. N. R.; Cronin, B.; Devine, A. L.; Dixon, R. N.; Nix, M. G. D. *Science* **2006**, *312*, 1637–1640.

(67) Devine, A. L.; Cronin, B.; Nix, M. G. D.; Ashfold, M. N. R. *J. Chem. Phys.* **2006**, *125*, 184302.

(68) An analysis of a microwave spectrum (ref 44) suggests that a free energy difference between 1*H*-1,2,3-triazole and 2*H*-1,2,3-triazole is 4.5 kcal mol<sup>-1</sup> at room temperature. B3LYP/6-311++G(d,p) calculations predict the free energy difference to be 3.8 kcal mol<sup>-1</sup>.

(69) Taft, R. W.; Anvia, F.; Taagepera, M.; Catalan, J.; Elguero, J. *J. Am. Chem. Soc.* **1986**, *108*, 3237–3239.

(70) Mackie, J. C.; Colket, M. B.; Nelson, P. F. *J. Phys. Chem.* **1990**, *94*, 4099–4106.

(71) Doughty, A.; Mackie, J. C. *J. Chem. Soc., Faraday Trans.* **1994**, *90*, 541–548.

(72) Kiefer, J. H.; Zhang, Q.; Kern, R. D.; Yao, J.; Jursic, B. *J. Phys. Chem. A* **1997**, *101*, 7061–7073.

(73) Barckholtz, C.; Barckholtz, T. A.; Hadad, C. M. *J. Am. Chem. Soc.* **1999**, *121*, 491–500.

(74) The small beam current for the *m/z* 40 ions obtained in the flowing afterglow-photoelectron spectroscopic experiment contrasts with the results

of the FA-SIFT measurements where the *m/z* 40 ions account for about one third of the product ions. The B3LYP/6-311++G(d,p) calculations predict that the gas-phase acidity of ketenimine to be 369.0 kcal mol<sup>-1</sup> at the C-H site. Because the gas-phase acidity of 1*H*-1,2,3-triazole is calculated to be 334.8 kcal mol<sup>-1</sup>, collisions of the ketenimine anion with the neutral triazole are expected to efficiently quench the ion through proton transfer.

(75) Ruscic, B.; Wagner, A. F.; Harding, L. B.; Asher, R. L.; Feller, D.; Dixon, D. A.; Peterson, K. A.; Song, Y.; Qian, X. M.; Ng, C. Y.; Liu, J. B.; Chen, W. W. *J. Phys. Chem. A* **2002**, *106*, 2727–2747.

(76) Kauer, J. C.; Sheppard, W. A. *J. Org. Chem.* **1967**, *32*, 3580–3592.

(77) Rochat, A. C.; Olofson, R. A. *Tetrahedron Lett.* **1969**, 3377–3380.

(78) Raap, R. *Can. J. Chem.* **1971**, *49*, 2139–2142.

(79) Green, S.; Herbst, E. *Astrophys. J.* **1979**, *229*, 121–131.

(80) Jacox, M. E.; Milligan, D. E. *J. Am. Chem. Soc.* **1963**, *85*, 278–282.

(81) Jacox, M. E. *Chem. Phys.* **1979**, *43*, 157–172.

(82) Rodler, M.; Brown, R. D.; Godfrey, P. D.; Tack, L. M. *Chem. Phys. Lett.* **1984**, *110*, 447–451.

(83) Rodler, M.; Brown, R. D.; Godfrey, P. D.; Kleibomer, B. *J. Mol. Spectrosc.* **1986**, *118*, 267–276.

(84) Buschek, J. M.; Holmes, J. L.; Lossing, F. P. *Org. Mass Spectrom.* **1986**, *21*, 729–731.

(85) Ito, F.; Nakanaga, T.; Sugawara, K.; Takeo, H.; Sugie, M.; Matsumura, C.; Hamada, Y. *J. Mol. Spectrosc.* **1990**, *140*, 177–184.

(86) Kroto, H. W.; Matti, G. Y.; Suffolk, R. J.; Watts, J. D.; Rittby, M.; Bartlett, R. J. *J. Am. Chem. Soc.* **1990**, *112*, 3779–3784.

(87) Lovas, F. J.; Hollis, J. M.; Remijan, A. J.; Jewell, P. R. *Astrophys. J.* **2006**, *645*, L137–L140.

(88) Vij, A.; Pavlovich, J. G.; Wilson, W. W.; Vij, V.; Christe, K. O. *Angew. Chem., Int. Ed.* **2002**, *41*, 3051–3054.

(89) Nguyen, M. T.; Ha, T. K. *Chem. Phys. Lett.* **2001**, *335*, 311–320.